AN ABSTRACT OF THE THESIS OF

MICHAEL Mc CALL GILBERT for the DOCTOR OF PHILOSOPHY
(Name) (Degree)

in CHEMISTRY presented on May 10, 1971
(Major) (Date)

Title: CONFORMATIONAL ANALYSIS: THE MOLECULAR STRUCTURE OF TETRAFLUOROHYDRAZINE, N_2F_4, BY GASEOUS ELECTRON DIFFRACTION

Abstract approved: Redacted for Privacy
Kenneth Hedberg

The molecular structure of tetrafluorohydrazine, N_2F_4, has been investigated by gaseous electron diffraction at a nozzle temperature of 25°C. Two models, one of a pure trans component and the other a mixture of gauche and trans components, give an acceptable fit to the data, but that for the mixture appears to be significantly better based on statistical criteria. The bond lengths and valence angles are essentially the same for the two models, except of course for the dihedral angle which is not a parameter in the pure trans model. The preferred model is the mixture with the two rotameric isomers (gauche with molecular symmetry C_2 and trans with symmetry C_{2h}) present in the approximate proportion 30% gauche/70% trans having essentially the same structure except for the dihedral angle. This suggests that the trans rotamer is 700-1200 cal/mole

more stable than the gauche. The bond lengths, valence angles, and root-mean-square amplitudes of vibration are (parenthesized values are 2σ): N-N = 1.492 Å (0.007), N-F = 1.372 Å (0.002), $\angle$FNF = 103.1° (0.6), $\angle$NNF = 101.4° (0.4), the dihedral angle in the gauche rotamer θ = 64.2° (3.7), ℓ_{N-N} = 0.048 Å (0.005), ℓ_{N-F} = 0.044 Å (0.002), $\ell_{F_1F_2}$ = 0.064 Å (0.004), $\ell_{N_1F_3}$ = 0.081 Å (0.008), $\ell_{F_1F_3}$ = 0.093 Å (0.012), and $\ell_{F_1F_4}$ = 0.079 Å (0.008). It is shown that the data are relatively insensitive to the amount of gauche rotamer present.

Conformational Analysis: The Molecular Structure of Tetrafluorohydrazine, N_2F_4, by Gaseous Electron Diffraction

by

Michael McCall Gilbert

A THESIS

submitted to

Oregon State University

in partial fulfillment of
the requirements for the
degree of

Doctor of Philosophy

June 1971

APPROVED:

Redacted for Privacy

Professor of Chemistry

in charge of major

Redacted for Privacy

Redacted for Privacy

Chairman of Department of Chemistry

Redacted for Privacy

Dean of Graduate School

Date thesis is presented May 10, 1971

Typed by Clover Redfern for Michael McCall Gilbert

ACKNOWLEDGMENT

I would especially like to thank cand. real Grete Gunderson for her guidance, assistance, and patience during the course of this investigation.

My sincere appreciation goes to my major professor Kenneth Hedberg for the wisdom and humor he has shown in guiding this investigation.

For her continued patience and encouragement throughout this research project, I thank my wife, Kathy.

Finally, I am grateful to the Oregon State University Computer Center for the grants of computing funds and for the excellent computing and support facilities they have provided.

TABLE OF CONTENTS

LIST OF FIGURES

LIST OF TABLES

CONFORMATIONAL ANALYSIS: THE MOLECULAR STRUCTURE OF TETRAFLUOROHYDRAZINE, N_2F_4, BY GASEOUS ELECTRON DIFFRACTION

INTRODUCTION

Tetrafluorohydrazine was first reported by Colburn and Kennedy (1958). Since then there have been many experimental studies of the structure of this compound, the results of which were in considerable disagreement in respect to the possible gauche-trans rotameric composition. The first study was on the microwave spectrum (Lide and Mann, 1959). Their data were consistent with a hydrazine-like model (point group C_2) for N_2F_4, and assuming bond distances of N-N = 1.47 Å and N-F = 1.37 Å, they found $\angle$FNF = 108°, $\angle$NNF = 104°, and a dihedral angle of 65°; the estimated accuracy was two to three degrees. The trans rotamer of N_2F_4 has C_{2h} symmetry and does not contribute to the microwave spectrum, but from intensity considerations they felt that the observed gauche species was present in concentrations of at least 10%. A minimum value for the barrier to internal rotation of 3 kcal/mole was given.

In 1963 both infrared (Durig and Lord, 1963) and Raman (Kutov and Tatevskii, 1963) spectra were reported. The infrared work included a fairly complete analysis carried out on the assumption that the molecule belonged to the point group C_2. The Raman assignments

contained some disagreements but it was concluded that the presence of significant amount of the trans rotamer was improbable.

An electron-diffraction study reported by Bohn and Bauer (1967) led them to flatly exclude a trans structure; they report the molecule to have the gauche conformation with parameter values $r(N\text{-}N) = 1.530$ Å (0.027), $r(N\text{-}F) = 1.393$ Å (0.008), $\angle FNF = 103.7°$ (0.8), $\angle NNF_1 = 99.0°$ (1.8), $\angle NNF_2 = 103.5°$ (2.1), and the dihedral angle $\theta = 69.3°$ (4.7). For the distances, these errors are approximately given by $[9\sigma_{LS}^2 + (0.005r)^2]^{1/2}$, and for the angles by $3\sigma_{LS}$. Shortly before, a low-temperature NMR investigation of N_2F_4 (Colburn, Johnson, and Haney, 1965) led to the conclusion that two rotational species, trans and gauche, were present and that the two differed in energy by about 100 to 200 cal/mole. In their paper, Bohn and Bauer (1967) stated that another explanation must be found for this result.

Recent Raman and infrared investigations substantiate the NMR investigation and also show that the earlier infrared and Raman spectra can be reassigned in terms of the presence of two rotamers. Durig and Clark (1968) compared their low-temperature Raman spectra with the infrared spectra of Durig and Lord (1963) and found the mutual exclusion principle to operate for a number of vibrational bands; their conclusion was that an appreciable amount of trans-N_2F_4 must be present, even at -120°C. Their assignment of the observed

bands is based on the assumption of an equilibrium of the trans and gauche rotamers. Koster and Miller (1968) investigated the infrared spectrum of the liquid at -120°C and found it to be essentially identical to that of the solid and the vapor. The mutual exclusion of a number of frequencies observed in the infrared and Raman spectra was taken as evidence for the presence of the trans rotamer in addition to the gauche one. The two isomers appeared to have approximately equal energies.

A more recent investigation of the gas-phase vibrational spectrum of N_2F_4 has been carried out by Oskam, Elst, and Duinker (1970). A number of new details on band positions and infrared band contours are reported and the vibrational assignments, based on the new infrared data and earlier reported Raman data, again strongly support the idea that N_2F_4 actually consists of an equilibrium mixture of two rotamers, trans and gauche, differing very little in energy as suggested by the NMR data.

As a consequence of this additional evidence, Cardillo and Bauer (1969) reinvestigated the structure of N_2F_4 by gaseous electron diffraction and arrived at a composition of 47% gauche - 53% trans rotamer. The temperature of the gas jet was estimated to be about 200°K, and this together with the reported composition, suggests that the trans rotamer is about 300 cal/mole more stable than the gauche rotamer. The parameter values and quoted error limits for the work

of Cardillo and Bauer are included in Table 3.

Between the period of the first and second reports from Professor Bauer's laboratory, we have initiated and essentially completed an electron-diffraction investigation of tetrafluorohydrazine. Our reasons for taking up the problem were to investigate the barrier to internal rotation and to compare the seemingly very long N-N bond distance reported by Bohn and Bauer and the even longer N-N bond distance in N_2O_4 which was currently being reinvestigated in this laboratory (McClelland and Hedberg, 1971).

Our preliminary work indicated the original gauche rotamer interpretation by Bohn and Bauer was incorrect and the electron-diffraction data we had collected were consistent with the recent Raman and infrared work; therefore a thorough investigation was carried out to determine the structure and mole ratios of the N_2F_4 rotamers.

SCATTERING THEORY

Since scattering theory applicable to gaseous electron diffraction has been presented by many authors (Brockway, 1936; Glauber and Schomaker, 1953; Mott and Massey, 1965; Seip, 1967), there seems to be no need for more than a brief summary here. The following is essentially the development of Seip.

The scattering or diffraction observed when a beam of high energy electrons is passed through a gaseous sample consists of both elastically scattered electrons, which are important for molecular structure determination, and inelastically scattered electrons, which are not.

In the case of elastic scattering, a single atom is treated and then an array of atoms having fixed relative positions (a molecule). In the most simple treatment, a single atom is represented by a spherically symmetric force field in which the potential energy of the scattered electrons is different from zero. The distribution of the scattered electron is assumed to be observed at large distances from the scattering centers, and an asymptotic solution is sought. A brief summary of the problem follows.

Let the scattering center be at the origin of the coordinate system and the incident beam be along the z axis. We assume the interaction between the electrons in the beam to be negligible. The Schrödinger equation for one electron is then

$$\nabla^2\psi(r) + 2m/\hbar^2[E-V(r)]\psi(r) = 0. \qquad (1)$$

∇^2 is the Laplace operator, m is the mass, E the energy of the electron, and $V(r)$ is the potential energy of the electron in the force field. By introducing $k^2 = 2mE/\hbar^2$[$k = p/\hbar = 2\pi/\lambda$, where λ is the electron wavelength], and $U(r) = 2m/\hbar^2 V(r)$, the expression becomes

$$\nabla^2\psi + [k^2 - U(r)]\psi = 0. \qquad (2)$$

The wave function for the incident electron is $\approx e^{ikz}$. The asymptotic form of the scattered wave is easily expressed in polar coordinates [r, θ, ϕ where θ is measured from the z axis]. The scattered wave spreads radially outward from the origin and cannot be a function of ϕ because of the assumed symmetry. Thus, since the intensity must decrease as $1/r^2$, we obtain $A(\theta)e^{ikr}/r$ for large r. The asymptotic form of the acceptable solution must therefore be

$$\psi^{\infty} = C[e^{ikz} + \frac{1}{r}A(\theta)e^{ikr}] \qquad (3)$$

where C is a normalization constant. By substitution of this solution into the Schrödinger equation it is seen that ψ^{∞} really satisfies the equation for large r values. Since the intensity is given by $|\psi|^2$, we find that the incident intensity is

$$I_o = |Ce^{ikz}|^2 = |C|^2 \qquad (4)$$

and the intensity of the radially outgoing scattered wave is found to be

$$I = (I_o/r^2)|A(\theta)|^2. \tag{5}$$

Our problem reduces therefore to the determination of the scattering amplitude $A(\theta)$.

The most popular method currently in use for the determination of the scattering amplitudes is that of partial waves, first introduced in scattering theory by Faxen and Holtsmark (1927). The result of solving the Schrödinger equation (Equation 2) by this method results in

$$A(\theta) = \sum_{l=0}^{\infty} \frac{(2l+1)}{2ik} P_l(\cos\theta)[e^{2i\delta_l} - 1] \tag{6}$$

where P_l is the Legendre polynomial of degree l and δ_l is the phase shift in the l'th partial wave.

To be able to carry out the summation, δ_l must be known. A number of methods for determining these terms have been devised (Schiff, 1965; Karle and Bonham, 1964; Peacher, 1965; Cox, 1967), all of which make use of approximate solutions to partial differential or integral equations. The best values of the scattering factors currently available are determined by numerical solutions of a combination of the different approximate expressions available for δ_l,

each used in the range where its accuracy is greatest.

An important approximation often utilized in this treatment is due to Born (Mott and Massey, 1965), and amounts to an assumption that inside the atom the amplitude of the incident wave is much greater than that of the scattered wave. Further, it is assumed that no phase shift occurs in the scattering process. The solution for a molecule, obtained by summing the scattered waves due to the atoms, is averaged over all possible orientations in order to account for the random phase relations between the waves scattered by different molecules.

Theories have been developed for the scattering factors of atoms that do not make use of a spherically symmetric force field, and also for molecules without the independent atom approximation. Unfortunately, these expressions do not readily yield useful solutions and we must await future developments for scattering theory to give us more accurate scattering factors for use in molecular structure determination.

In lieu of a more exact form of the expression for the intensity of electrons scattered by a molecule, the following treatment is used. We apply the complex scattering amplitudes (Equation 6), but still regard the atoms as independent scattering centers. The intra-atomic multiple scattering is neglected. The difference in phase caused by the difference in path length between a wave scattered from atom i and a wave scattered from the origin is $\mathbf{R}_i \cdot \mathbf{S}$. Let us first consider

a rigid molecule in a fixed orientation. The scattered intensity is then (leaving out the multiplier I_o/r^2):

$$\sum_{i,j} A_i^* e^{-i\mathbf{S}\cdot\mathbf{R}_i} A_j e^{i\mathbf{S}\cdot\mathbf{R}_j} \tag{7}$$

where $\mathbf{R}_i$ gives the position of atom i. If the average over random orientations is considered, then

$$I(s) \simeq \sum_{i,j} A_i^* A_j \frac{\sin(R_{ij}s)}{R_{ij}s} \tag{8}$$

where R_{ij} is the distance between atom i and j. This may be written in a more usable form as

$$I(s) = \sum_{i<j} |A_i||A_j| \cos(\eta_i - \eta_j) \frac{\sin(R_{ij}s)}{R_{ij}s} \tag{9}$$

where

$$A(s) = |A(s)| e^{i\eta(s)}. \tag{10}$$

While this expression is adequate for a rigid molecule, we must change the expression to account for molecular vibrations. If $P_{ij}(R)dR$ gives the probability that the distance between atoms i and j is between R and R + dR, then we can write

$$I(s) = \sum_{i<j} A_i A_j \cos \Delta\eta_{ij} \int P_{ij}(R) \frac{\sin(Rs)}{Rs} dR \,. \qquad (11)$$

We usually assume a Gaussian distance distribution, corresponding to a harmonic oscillator potential function, of the form

$$P_{ij}(R) = \frac{1}{\sqrt{2\pi}} \frac{1}{\ell_{ij}} \exp\left(-\frac{(R-R_{ij})^2}{2\ell_{ij}^2}\right) \qquad (12)$$

where ℓ_{ij} is the root-mean-square amplitude of vibration, and R_{ij} now denotes the mean distance between atoms i and j. From this, we obtain to a very good approximation

$$I(s) = \sum_{i<j} A_i A_j \cos \Delta\eta_{ij} \exp\left(-\frac{1}{2}\ell_{ij}^2 s^2\right) \frac{\sin r_{ij} s}{r_{ij} s} \,. \qquad (13)$$

Here r_{ij} is equal to $R_g(1)$ (Bartell, 1955) which is the center of gravity of the function $P(r)/r$. It is this value which shall be referred to as the internuclear distance henceforth.

THE FOURIER TRANSFORM AND SPECTRAL ANALYSIS METHODS

The intensity expression given in Equation 11 suggests that it is approximately the Fourier sine transform of a sum of Gaussian probability functions. This relation can be used in finding the inverse transform which gives a distribution of distances and estimates of the root-mean-square amplitudes of vibration for the molecule studied. To carry out the transform process, the following conditions are usually necessary:

1) The coefficients $A_i A_j \cos \Delta\eta_{ij}$ must be transformable into essentially constant coefficients which are proportional to $Z_i Z_j$, where Z_i is the atomic number of atom i.
2) The intensity curve with constant coefficients is multiplied point by point by s.
3) The intensity curve, called I'(s), is multiplied by a damping function, $\exp(-Bs^2)$, to account for the finite series length. B is usually chosen such that $\exp(-Bs_{max}^2) \approx 0.1$.

The intensity function is now written approximately as

$$I'(s) = \sum_{i<j} Z_i Z_j e^{-\frac{\ell_{ij}^2 s^2}{2}} r_{ij}^{-1} \sin(r_{ij} s) \qquad (14)$$

and the Fourier transform of this may be written as

$$D(r) = 2/\pi \int_0^{S_{max}} I'(s) e^{-Bs^2} \sin(rs) ds \qquad (15)$$

The peaks which appear in the curve $D(r)$ can be interpreted as follows. Each peak, assuming it is not a composite made up from more than one internuclear distance, will have an area which is proportional to $n_{ij} Z_i Z_j / r_{ij}$, there n_{ij} is the number of times distance r_{ij} occurs in the molecule. The spread or broadness of each peak is a function of both the mean-square amplitude of vibration of the atoms i and j and the damping factor B. This is summarized by the expression

$$D(r) = \frac{1}{\sqrt{2\pi}} \sum_{i \neq j} \frac{Z_i Z_j}{r_{ij}} \frac{1}{\sqrt{\ell_{ij}^2 + 2B}} \exp\left[- \frac{(r - r_{ij})^2}{2\ell_{ij}^2 + 4B} \right] . \qquad (16)$$

While the radial distribution method is certainly the most straight-forward and useful method of examining electron-diffraction data for distance distributions, other methods of spectral analysis are also applicable under certain conditions. Some of these methods were examined in the course of this study and will be briefly summarized here.

The autocorrelation function $A(\tau)$ of a function $I(s)$ may be

defined as

$$A(\tau) = \int_{-\infty}^{\infty} I(s)I(s-\tau)ds \tag{17}$$

and is simply the mean value of the product $I(s)I(s-\tau)$ over the range of the variable s. Therefore the variable $A(\tau)$ characterizes the relationship between values of the function $I(s)$ separated by an amount τ on the s scale of the variable; theoretically $A(\tau)$ contains all of the information found in $I(s)$, only in an averaged form.

The autocorrelation function $A(\tau)$ is related to its power spectrum $APS(r)$ through a pair of Fourier transforms (Jenkins and Watts, 1968). These relationships are expressed as

$$APS(r) = \frac{1}{\sqrt{2\pi}} \int_{-\infty}^{\infty} A(\tau)e^{-ir\tau}d\tau \tag{18}$$

and

$$A(\tau) = \frac{1}{\sqrt{2\pi}} \int_{-\infty}^{\infty} APS(r)e^{ir\tau}dr\,. \tag{19}$$

Since the autocorrelation function $A(\tau)$ is an even function, its Fourier transform is also even, and we can write

$$APS(r) = \sqrt{\frac{2}{\pi}} \int_{0}^{\infty} A(\tau)\cos(r\tau)d\tau\,. \tag{20}$$

In a like fashion we can derive a cross-correlation function between $I(s)$ and a test function $t(s)$. Here

$$CR(\tau) = \int_{-\infty}^{\infty} I(s)t(s-\tau)ds \tag{21}$$

and the Fourier transform pairs are

$$CRPS(r) = \frac{1}{\sqrt{2\pi}} \int_{-\infty}^{\infty} CR(\tau)e^{-ir\tau}d\tau \tag{22}$$

and

$$CR(\tau) = \frac{1}{\sqrt{2\pi}} \int_{-\infty}^{\infty} CRPS(r)e^{ir\tau}d\tau . \tag{23}$$

When it is taken into account that electron-diffraction data are not available over an infinite interval but only for a small range of s and the expressions are modified accordingly (Fano, 1950; Schroeder and Atal, 1962), and account is also taken of the fact that $I(s)$ is a sum of sine waves which vanish at the origin and $I(s) = I(-s)$, we can write modified expressions as

$$A(\tau) = 2a \int_{0}^{S_m} I(s)I(s-\tau) \exp[-2a(S_m - s)]ds \tag{24}$$

and

$$APS(r) = 2 \int_{0}^{\tau_m} A(\tau) \exp(-a\tau) \cos(r\tau)d\tau \tag{25}$$

where S_m is the maximum value of s for which data exists, and α is chosen so that $\exp(-2\alpha S_m) \approx 0$. Also for the cross-correlation function

$$CR(\tau) = 2\alpha \int_0^{S_m} I(s)t(s-\tau) \exp[-2\alpha(S_m - s)]ds \tag{26}$$

and

$$CRPS(r) = 2 \int_0^{\tau_m} CR(\tau) \exp(-\alpha\tau) \cos(r\tau)d\tau . \tag{27}$$

If a series of cross-correlation functions and the corresponding spectra are computed, a two-dimensional power spectrum can be plotted from the resulting data. The r values of the test function [a simple sine function of the form $t(s) = \text{const.} \cdot \sin(rs)$] is varied over a certain range of interest, depending on where internuclear distances are expected to be found. All maxima corresponding to internuclear distances are located along the diagonal of the two-dimensional power spectrum. It is therefore sufficient to compute the terms along the diagonal to obtain the necessary structure information. The diagonal terms will be referred to as the diagonal power spectrum (DPS).

One of the very useful properties of these kinds of functions is that of filtering out random errors from experimental functions. To

show this we represent a periodic function as $f(t)$ and a function of random or white noise as $n(t)$. Then the experimental observed function, $q(t)$, is represented as

$$q(t) = f(t) + n(t). \tag{28}$$

The autocorrelation function is then given by

$$a(\tau) = \langle [f(t)+n(t)][f(t-\tau)+n(t-\tau)] \rangle,$$

which reduces to

$$a(\tau) = \langle f(t)f(t-\tau) \rangle + \langle f(t)n(t-\tau) \rangle + \langle n(t)f(t-\tau) \rangle + \langle n(t)n(t-\tau) \rangle .$$

If there is no correlation between the periodic signal and the random errors, then we can see that

$$\langle q(t)q(t-\tau) \rangle = \langle f(t)f(t-\tau) \rangle . \tag{29}$$

Another method of examining the intensity function for its distance (i.e. frequency) distribution is that of averaging complex demodulates. If $I(s)$ is our intensity function which extends to S_m, and we have a series of weights w_k which form a symmetrical low-pass filter of length $2N-1$, then the complex demodulates at distance r is the complex series

$$Z_s(r) = \sum_{\tau=1-N}^{N-1} w_\tau I(s+\tau) \exp[-ir(s+\tau)] \tag{30}$$

for

$$s = N-1, N, N+1, \ldots, S_m - N.$$

These $S_m - 2(N-1)$ complex values at distance r are averaged to form the spectral estimate

$$C(r) = \frac{1}{S_m - 2(N-1)} \sum_{s=N-1}^{S_{m-N}} |Z_s(r)|^2. \tag{31}$$

What is being computed is roughly as follows. Moving segments of $I(s)$ of length $2N-1$ are shifted in frequency so that the distance of interest r_o corresponds to frequency zero. A low-pass filter is applied to cut off frequencies corresponding to distances other than r_o. The spectrum at r_o is calculated and the average of these over all segments gives an estimate of the power at r_o. The only filter which has been examined in this work is the Tukey or Cosine filter which can be expressed as

$$w_k = \frac{1}{2}\{1 + \cos(\frac{\pi k}{N})\} \tag{32}$$

where $k = 0, 1, 2, \ldots, N-1$. While there is reason to believe that more modern filter designs could give much improved results, these

have not yet been tested.

One further function which was examined is the sharpened radial distribution curve (SRD). According to definition, the function is computed as the sine transform of the molecular intensity function modified by a function $g(s) = \sqrt{2\lambda}\ \exp[-\lambda(S_m - s)]$. In the Fourier sine transform of this function $g(s)I(s)$, each internuclear distance contributes with a Gaussian function that is sharpened by multiplication with a cosine function whose maximum value coincides with the maximum of the Gaussian peak. The amount of sharpening is determined by the period of the cosine function which is again a function of λ. An increase in λ leads to an increased sharpening effect; however an increase in peak sharpening is also accompanied by a corresponding increase in series-termination effects which may easily offset any resolution gained in sharpened peaks. The sharpened radial distribution function has the form

$$SRD(r) = \sqrt{2\lambda} \int_0^\infty I(s)\ \exp[-\lambda(S_m - s)]\ \sin(rs)ds. \qquad (33)$$

EXPERIMENTAL

A sample of tetrafluorohydrazine was obtained from Air Products and Chemicals, Inc., Allentown, Pennsylvania. The stated purity of this material was greater than 99.9% and it was used without further purification. Electron diffraction photographs were made in the Oregon State apparatus using a rotating sector with angular opening approximately proportional to r^3, 8 in x 10 in and 5 in x 7 in Kodak process plates, beam currents of 0.2 to 0.7 μa, and exposure times of 15-180 sec. The sample container, connected directly to the diffraction apparatus using a Kel-F lubricated joint, was cooled to -130°C to obtain a suitable vapor pressure. The nozzle temperature was 25°C and the ambient pressure in the apparatus during the exposures was about 2×10^{-5} Torr. The electron wavelengths were in the range 0.05697-0.05743 Å, as determined by measurements of the accelerating voltage calibrated from diffraction patterns of gaseous CO_2. Nozzle-to-plate distances were 75.08, 29.96, and 12.36 cm.

Twenty-one diffraction plates were found to be free from defects and of proper quality and density. The plates were scanned along a diametrical line on a modified Joyce-Loebl microdensitometer while being rotated about the axis of the rings. The output of this double-beam instrument, normally a chart record of photograph density as a

function of distance on the specimen, was digitized by fitting a potentiometer with external power supply to the pen mechanism to provide a voltage proportional to density. This voltage is conveyed to a system of a voltage-to-frequency converter, a five-digit counter, and a digital punch and recorded to five figures. The stability of this system is better than two parts in ten thousand or 0.02%. Interval sampling is achieved by repeated activation of a microswitch with a cam fixed to a screw made to drive the specimen table; the microswitch initiates counting which continues for a pre-set time, usually one second. Digitized data were obtained at intervals of 0.3514 mm on the plate. During acquisition of the counts comprising each datum, the plate was rotated exactly two cycles and translated 0.1171 mm; thus each measurement reflected an integration over a path of the plate several centimeters long. In the process of scanning the plates it was found that at least 15 of the plates were of very good quality and the data collected would be acceptable for structure determination and refinement.

The plate scans were recorded in counts per second on an arbitrary scale which was then related to a density scale by scanning a standard step wedge calibrated in optical density units. The step wedge was scanned following the scan of each plate with all instrument settings unchanged. All of the curves were transferred from paper tape to computer files and stored for use in the data reduction

program

The data were reduced (Hedberg and Iwasaki, 1962) using a computer program written by Lise Hedberg which performed the following calculations:

1. The curves in counts were converted to density units.
2. The precise center of each scan was determined by finding the minimum sum-of-squares deviation for the two branches of the curves.
3. The s-vector corresponding to the points on the curve was calculated and interpolated for even intervals of s. (Note: $s = 4\pi\lambda^{-1} \sin\theta$, where 2θ is the scattering angle and λ is the electron wavelength calculated from the relativistically corrected voltage.)
4. The geometrical corrections were applied to the intensities. If density units on the plates are designated $I_p(s)$, the expression for the total corrected intensity is

$$I_t(s) = \frac{I_p(s) \cdot H^3 \cdot 10^{-8}}{a(s) \cos^3 2\theta}, \qquad (34)$$

where $a(s)$ is the sector function and H^3 is the cube of the camera height. (H^3 scales the data to correct for the different sector functions applied at different heights.)
5. $I_t(s)$ was then multiplied by s^4 which gave curves called 'sector corrected curves' described by

$$s^4 I_t(s) = kI_m(s) + B_{exp}(s), \tag{35}$$

where $I_m(s)$ is the molecular intensity and $B_{exp}(s)$ is the experimental background intensity. The scale factor k arises from the fact that the intensities are not measured on an absolute scale.

6. The results from the left and right sides of the diametrical scan line were averaged.

The results from each plate were plotted and eight curves, three from the long distance, three from the middle distance, and two from the short distance, were selected as those being most free of noise and defects. Smooth backgrounds were then fitted to each of these. These curves are shown in Figure 2 and the experimental conditions for each are given in Table 1.

After subtracting out smooth background curves in the usual manner, the resulting curves were multiplied by s. The results are called $sI_m(s)$ curves and have a form corresponding to

$$sI_m(s) = \sum_{i \neq j}' n_{ij} A_i A_j r_{ij}^{-1} V_{ij}(s) \cos |\Delta\eta_{ij}(s)| \sin(r_{ij} s) \tag{36}$$

which is seen to be very similar to Equation 13. The A_i's are modified electron scattering amplitudes, r_{ij}'s unique internuclear

distances, n_{ij}'s multiplicities of distances r_{ij}, V_{ij}'s molecular vibration factors, and $\Delta\eta_{ij}$'s phase differences. The scattering amplitudes A_i and the phases η_i used in the structure determination were obtained from Cox and Bonham's (1967) table as follows. The amplitude values tabulated at 70 and 40 kV were first linearly interpolated to give values corresponding to the accelerating voltage. These values were then interpolated to give values at intervals $\Delta s = 0.25$ by fitting a cubic equation to four points, two on each side of the desired point. Finally, the array of values was multiplied by s^2 and the results smoothed. The phases were obtained by interpolating the values tabulated at 10, 40, 70, and 100 kV according to a cubic equation followed by a similar interpolation to give values at intervals $\Delta s = 0.25$. Subsequent smoothing was felt not to be necessary.

The ranges of the data from the 75-, 30-, and 12-cm camera distances were $1 < s < 13$, $6 < s < 31$, and $22 < s < 45$, respectively, and the data interval was $\Delta s = 0.25$. These curves are shown in Figure 3, and the data given in Table 2.

PRELIMINARY STRUCTURE ANALYSIS

For the purpose of calculating radial distribution curves, a composite intensity curve was made by scaling and averaging the individual curves in the overlap regions. The composite intensity curve was then converted into one with essentially constant coefficients $[I'_m(s)]$ by multiplying each point by $(Z_N Z_F / A_N A_F)$.

A preliminary experimental radial distribution curve was first calculated according to

$$D(r) = \frac{2\Delta s}{\pi} \sum_{s=1}^{S_{max}} I'_m(s) \exp(-Bs^2) \sin(rs) \qquad (37)$$

using $B = 0.0012\ \text{Å}^2$ to assure a minimum of series termination errors. A theoretical intensity curve was then calculated using the parameter values suggested by the preliminary $D(r)$ curve; the results were scaled to the experimental curve by a least-squares procedure and used to make small background corrections in the observed intensity curve and to supply the missing intensity data in the range $0 < s < 1$. The radial distribution curve was then recalculated using data over the range $0 < s < 45$. The final radial distribution curve shown in Figures 5 and 6 reflects additional small background changes in the intensity curve introduced in the course of the

refinement.

The positions of the four peaks of the radial distribution curve could be interpreted in terms of either a gauche or trans rotamer of N_2F_4 having the following distances: 1.37 Å, N-F; 1.50 Å, N-N; 2.15 Å, F_1F_2; 2.25 Å, N_1F_3 (and F_2F_4 non-bond distance for the gauche rotamer); 2.60 Å, F_1F_3 non-bond distances (trans rotamer) and F_1F_4 non-bond distances (gauche rotamer); 3.35 Å, F_1F_4 non-bond distances (trans rotamer) and F_1F_3 non-bond distance (gauche rotamer). Considerations of the relative areas of the peaks at 2.60 and 3.35 Å indicated that the D(r) curve could not be interpreted in terms of only a gauche rotamer being present. It was not clear, however, whether a mixture of gauche and trans rotamers or a pure trans component would give the best fit to the observed data. This situation is due to the structure of the $-NF_2$ group: the angles are such that the F_1NF_2 angle projected along the N-N bond is close to 120°, so that projected N-F distances from different $-NF_2$ groups lie almost in a straight line, even in the gauche conformation.

The area of the isolated non-bond fluorine-fluorine peak at 3.35 Å is determined by the trans/gauche ratio, and can vary up to 50% on going from pure trans to pure gauche because the trans rotamer has two distances at this separation while the gauche has only one. Preliminary observations indicated that the trans rotamer was present in amounts greater than 50% and possibly as much as 100%.

The area of the 3.35 Å peak is somewhat affected by errors in the low-angle diffraction data and inaccuracies in the scattering factors used for low angles. Also, the base line may be slightly shifted, depending on the model used to calculate the inner peak of the intensity curve used to provide the missing experimental data. Hence it was necessary to investigate two models of the structure, one composed of a trans rotamer only, and one composed of a mixture of gauche and trans rotamers, and to closely examine the parameters, error limits, and radial distribution curves for each.

A number of power spectra were calculated in order to resolve the N-N peak at 1.50 Å from the N-F peak at 1.37 Å and also to see what information could be gained in the 2.1-2.7 Å region, i.e., to see whether or not the peak components could be better resolved in this region. The computational expressions used for these calculations are given in the Appendix.

All of the power spectra showed a peak at approximately 1.5 Å which was resolved from the strong peak at 1.37 Å, with the exception of the spectrum of complex demodulates. The sharpened radial distribution curve (SRD), which is shown in Figure 7, was calculated with a value of a equal to 0.03, and gives as good resolution as any of the averaging methods. It can be seen that series termination error is quite severe and that no additional information is gained in the region >2 Å over that given by a conventional radial distribution

curve. The autocorrelation power spectrum (APS) gives essentially the same information as the SRD in the region 1-2 Å. The best resolution was obtained with $\alpha = 0.02$ and $\tau_{max} = 40.0$. However, much of the higher frequency information is lost, as can be seen in the almost missing peaks in the regions of 2.6 and 3.4 Å. This is also true of the diagonal power spectrum, though not to as great an extent. The DPS gives about as good resolution as the SRD in the 1-2 Å region, but since it is much more complicated and time consuming to calculate, its use is questionable. These spectra are given as part of Figure 7.

The spectrum of complex demodulates, also shown in Figure 7, has very poor resolution. This is due to the lack of a sharp low-frequency filter which greatly reduces the resolution and also tends to smother the higher frequencies. The spectrum shown was calculated with a Tukey filter of 170 terms, $\tau_{max} = 42$, and is the best spectrum obtained. Other more complex filter designs were not tried.

The estimation of distance distributions using power spectra was not helpful in this study. While others (Traetteberg, 1964; Traetteberg and Bonham, 1965) have found these methods useful in resolving bond distances of nearly equal weight in the range 1-2 Å, separated by as little as 0.1 Å, the resolution of the N-N bond distance peak at 1.5 Å from the N-F bond distance peak at 1.37 Å was

accompanied by shifts in the apparent N-N bond distance of as much as 0.1 Å from its true value. Hence we could only find the true split between the N-F and N-N distances by comparing theoretical spectra with the experimental ones. For the structure analysis, this offered no advantage over what could be done with the least-squares method.

STRUCTURE REFINEMENT AND ERROR ESTIMATES

Refinements of the structures were carried out by the method of least-squares based upon intensity curves (Hedberg and Iwasaki, 1964) in the mathematical form defined by Equation 36 with the harmonic approximation $V_{ij}(s) = \exp[-<\delta\ell_{ij}^2>s^2/2]$, using a unitary weight matrix. The computer program is capable of operating with many sets of observed intensity data in place of just one set, such as is represented by a single composite intensity curve, and simultaneously adjusting estimates of the structural parameters and mole fractions of components of mixtures.

A part of the final results of the least-squares refinement gives the error matrix (Hedberg and Iwasaki, 1962; Ryan and Hedberg, 1969). The diagonal elements of the error matrix are estimates of σ_i^2, and reflect random errors not including the possible correlations among observations; the off-diagonal elements $\rho_{ij}\sigma_i\sigma_j$ allow calculation of the correlation of errors from the ρ_{ij}-coefficients. The error estimates given in this investigation are

$$2\sigma_r = 2[2\sigma_{LS}^2 + (0.0005)^2]^{1/2} \tag{38}$$

$$2\sigma_\ell = 2[2\sigma_{LS}^2 + (0.02\ell)^2]^{1/2} \tag{39}$$

$$2\sigma_a = 2[2\sigma_{LS}^2]^{1/2} \tag{40}$$

where the σ^2_{LS} are the diagonal elements of the error matrix and the factors 2, 0.0005, and 0.02 respectively take into account estimated correlations among observations, errors in wavelength, camera distance, and sector calibration, and error in conversion of photographic density to scattered electron intensity.

Two geometrical models of the molecule were involved in the interpretation of the experimental data. The trans rotamer (C_{2h}-symmetry) is described by four parameters: the N-N and N-F bond distances and the $F_1N_2F_2$ and $N_1N_2F_3$ valence angles (Figure 1) and has six different types of distances, each having a root-mean-square amplitude of vibration associated with it, giving a total of 11 independent parameters (scale constant included) to be adjusted by the least-squares refinement. The gauche rotamer (C_2-symmetry) is described by six parameters: the N-N and N-F bond distances, the $F_1N_1F_2$, $N_1N_2F_3$, and $N_1N_2F_4$ valence angles, and the dihedral angle (Figure 1); in addition there are eight root-mean-square amplitudes of vibration giving a total of 15 independent parameters.

The refinement based on a single trans component proceeded in a routine fashion. All of the 11 parameters converged to acceptable values. The final parameter values for this model with their associated errors are given in Table 3; theoretical intensity and radial distribution curves are shown in Figures 4 and 5, respectively, together with the corresponding differences between experimental and

theoretical curves. The correlation matrix is given in Table 5. Except for the slight area discrepancy for the 3.36 Å non-bonded F_1F_4 peak in the radial distribution curve, the refinement of this model gave a perfectly acceptable representation of the diffraction data judged by the usual quality standards.

A complete refinement of the trans/gauche mixture model would involve the simultaneous adjustment of 26 independent parameters. Although the two rotamers in principle are independent of each other, they are structurally similar, giving many overlapping distances. In order to increase the statistical significance of the refinement it was felt desirable to introduce the following constraints on the model:

1. The valence angles $N_1N_2F_3$ and $N_1N_2F_4$ in the gauche rotamer were assumed to be equal.
2. The valence angles were assumed to be equal in the two rotamers.
3. The bond distances (N-N and N-F), and their amplitudes of vibration in the gauche rotamer were assumed to be equal to the corresponding ones in the trans rotamer.
4. Additional restraints on the amplitudes of vibration were:

$$\ell_{F_1F_4(g)} = \ell_{F_2F_4(g)} = \ell_{F_1F_3(tr)} \quad \text{and} \quad \ell_{F_1F_3(g)} = \ell_{F_1F_4(tr)}.$$

These constraints reduce the number of adjustable parameters to 13,

including the composition and the scale constant. They are: the N-N and N-F bond distances, the $F_1N_1F_2$ and $N_1N_2F_3$ valence angles, the diehedral angle θ, the amplitudes $\ell_{N\text{-}N}$, $\ell_{N\text{-}F}$, $\ell_{F_1F_2}$, $\ell_{N_1F_3}$, $\ell_{F_1F_3(tr)}$, and $\ell_{F_1F_4(tr)}$, the mole fraction and a scale constant. The parameter values found for this model with associated errors are given in Table 3; theoretical intensity and radial distribution curves are shown in Figures 4 and 5 respectively along with the corresponding difference curves. The correlation matrix is given in Table 4.

A number of different starting models were used in the least-squares refinements and all with an initial mole fraction in the range of 0.5 to 0.9 for the trans rotamer converged to give parameter values within the standard error limits of those given in Table 3. Several refinements were attempted without constraints 1 and 2. The standard deviation in fitting the intensity curve increased with these additional parameters and the refinements would not converge but instead oscillated around this higher residual. Although there were only slight shifts in any of the valence angles (less than 0.5 degrees), high correlations between the distances and the corresponding amplitudes of vibration gave standard deviations which indicated that any apparent shift was probably meaningless. Attempts to carry out refinements with this same parameter set except for the mole fraction ratio held constant at 71% trans/29% gauche were also unsuccessful. Since the

differences which might exist among the valence angles appear to be smaller than the standard errors obtained with the assumption of no difference, and because of the very excellent agreement with observation provided by the constrained model, the results given in Table 3 for this model are felt to be as good a representation of the molecular structure as can be obtained from the data.

A comparison of the two different models, one a pure trans component and the other a mixture of trans and gauche rotamers, shows that the mixture is to be favored. The R-factor ratio test described by Hamilton (1964, p. 157-160) shows the trans/gauche mixture to produce a significantly better fit even at the 99% confidence level.

Least-squares refinements on both models were also carried out using a diagonal weight matrix (Hedberg and Iwasaki, 1964; Gundersen and Hedberg, 1969) calculated according to

$$P(s) = Hs^{-1} \exp(-bs^2)[1 - \exp(-as^2)] \qquad (41)$$

with $a = 0.02 - 0.03$ and $b = 0.0003 - 0.0004$, and H equal to the camera height (in cm) of each individual plate. These refinements gave essentially the same results, but with lower error limits. Since the refinements based on a unitary weight matrix gave results which do not differ from these by even the smaller error limits, the more conservative (larger error limits) results given by the use of the unitary weight matrix are preferred.

DISCUSSION

The electron-diffraction data can be interpreted in terms of either a pure trans component of tetrafluorohydrazine or a mixture of trans and gauche rotamers, due to their very similar structures. The best results are obtained by interpreting the data as a mixture, which is in agreement with the findings from NMR (Colburn, 1965), molecular spectroscopy (Durig, 1968; Koster, 1968; Oskam, 1970), and Cardillo and Bauer's electron-diffraction experiment (1969).

The agreement of this work with that of Cardillo and Bauer is excellent for all of the bond distances, valence angles, and amplitudes of vibration. While these authors chose to define their model with many more parameters (angles and vibrational amplitudes), essentially none of their values, and certainly not an average of these values, for any of the valence angles or non-bond amplitudes of vibration differ significantly from those determined here. The N-F and N-N bond distances determined from the independent studies agree to well within their standard errors.

It is clear from Figures 4 and 5 that the differences between a model of 100% trans N_2F_4 and one of 70% trans/30% gauche N_2F_4 are very slight as far as electron-diffraction intensity and radial distribution curves are concerned. The only major difference in the intensity curve appears in the region $s = 3\text{-}12$. This is not in agreement with

the study of Cardillo and Bauer (1969), which shows much larger differences in the intensity curve over most of the scattering region with small changes in the trans/gauche ratio. While the values of the molecular parameters are not significantly affected by this discrepancy, one must proceed cautiously in interpreting the electron-diffraction results as to the fractions of trans and gauche components present and in applying error limits to these values.

The difference in energy of the gauche and trans rotamers can be determined from the Boltzmann expression $N_i = g_i \exp(-E_i/kT)$ from a knowledge of the ratio of mole fractions of the two species $N_{(tr)}/N_{(g)}$ and the temperature of the gas at the point of diffraction, assuming the two components are at equilibrium. While there is some uncertainty in the mole fraction ratio as discussed above, the mean temperature of the gas at the nozzle tip differs negligibly from the temperature of the nozzle (Ryan and Hedberg, 1969). If the limits on the mole percent of the trans component are taken to be 60-80%, then the trans rotamer is 650 to 1250 cal/mole more stable than the gauche rotamer. The percent ratio 71% trans/29% gauche gives an energy difference of 946 cal/mole.

The N-F bond distance of 1.372 Å ($2\sigma = 0.002$) agrees well with the distance calculated from Schomaker-Stevenson radii and corrected for electronegativity difference (1.38 Å). The N-F distance and the valence angle $\angle F_1N_1F_2$ (103.1°; $2\sigma = 0.4°$) are very

close to the values N-F = 1.371 Å and $\angle$FNF = 103 ± 1° reported for NF_3 (Sheridan and Gordy, 1950). The N-N bond distance of 1.492 Å (2σ = 0.007) is significantly longer than that found in N_2H_4 (1.453 Å, Yamaguchi, et al., 1959) and other substituted hydrazines, a difference compatible with the much lower bond dissociation energy of N_2F_4 (20 kcal/mole) as compared to N_2H_4 (60 kcal/mole). Perhaps this type of correlation should not be pushed with N_2O_4 (dissociation energy 12.7 kcal/mole) because the planar N_2O_4 molecule certainly has much different bond properties than N_2F_4. However, it is at least satisfying that a very long N-N bond distance in N_2O_4 (1.78 Å, McClelland and Hedberg, 1971) does accompany an energy of dissociation even lower than N_2F_4.

Table 1. Data for electron-diffraction photographs used for the structure determination of gaseous N_2F_4.

Plate Identification	Plate Size [a]	Accelerating voltage (volts)	Wavelength [b] (Å)	Exposure (sec)	Beam Current (μa)	Density range	Nozzle-to-plate distance (cm)	s-range
I-101-06	5" x 7"	43882	0.057326	30	0.10	0.4-1.1	75.075	1.00- 7.75
I-104-08	8" x 10"	43829	0.057363	20	0.12	0.2-0.5	75.075	1.00-12.75
I-104-10	5" x 7"	43836	0.057358	15	0.12	0.1-0.3	75.075	1.00- 7.75
I-110-03	5" x 7"	43736	0.057426	180	0.16	0.7-1.8	29.961	6.00-19.50
I-110-04	8" x 10"	43753	0.057414	180	0.16	0.5-1.5	29.961	6.00-28.75
I-110-11	8" x 10"	43778	0.057397	150	0.12	0.4-1.0	29.961	6.00-31.25
I-214-24	5" x 7"	44414	0.056968	180	0.70	0.6-1.0	12.359	22.00-44.75
I-214-25	5" x 7"	44395	0.056981	120	0.70	0.5-0.9	12.359	22.00-44.75

Nozzle Temperature = 25°C Bath Temperature = -130°C Run-in Pressure = 2×10^{-5} Torr

[a] Kodak process plates.

[b] Wave-lengths were determined from the accelerating voltage which was calibrated against diffraction patterns of gaseous CO_2 (see Gundersen and Hedberg, 1969).

Table 2. Experimental intensity curves $[sI_m(s)]$ for N_2F_4.

s \ Δs	0.00	0.25	0.50	0.75
Long camera distance (75 cm) Plate I-101-06				
1.00	30	47	39	-10
2.00	-89	-203	-302	-339
3.00	-348	-285	-226	-218
4.00	-307	-487	-699	-698
5.00	-383	386	1488	2549
6.00	3082	2900	2015	644
7.00	-854	-2044	-2832	-3069
Long camera distance (75 cm) Plate I-104-08				
1.00	24	36	33	-7
2.00	-72	-158	-236	-261
3.00	-264	-234	-179	-168
4.00	-244	-399	-528	-592
5.00	-298	337	1151	2040
6.00	2506	2374	1620	508
7.00	-713	-1737	-2460	-2601
8.00	-2584	-2175	-1476	-567
9.00	487	1580	2345	2609
10.00	2369	1637	703	-197
11.00	-571	-540	-323	-247
12.00	-191	-484	-966	-1285
Long camera distance (75 cm) Plate I-104-10				
1.00	19	31	24	-7
2.00	-58	-125	-191	-214
3.00	-215	-190	-167	-157
4.00	-192	-305	-421	-439
5.00	-252	264	929	1602
6.00	2006	1895	1257	363
7.00	-528	-1292	-1788	-1982
Middle camera distance (30 cm) Plate I-110-03				
6.00	3126	2932	2016	652
7.00	-740	-1916	-2800	-3164
8.00	-3037	-2636	-1869	-863
9.00	383	1669	2705	3163
10.00	2714	1881	782	-189
11.00	-660	-707	-455	-237

(continued)

Table 2. Continued.

s \ Δs	0.00	0.25	0.50	0.75
12.00	-324	-719	-1249	-1701
13.00	-1814	-1787	-1466	-826
14.00	-32	998	2197	3053
15.00	3690	3341	2080	485
16.00	-1454	-2762	-3439	-3295
17.00	-2471	-1585	-711	-62
18.00	310	605	890	1150
19.00	1239	1164	1070	
Middle camera distance (30 cm) Plate I-110-04				
6.00	3126	2913	2013	718
7.00	-716	-1967	-2847	-3160
8.00	-3105	-2763	-2003	-967
9.00	395	1741	2799	3198
10.00	2728	1857	708	-234
11.00	-685	-720	-492	-333
12.00	-366	-731	-1234	-1624
13.00	-1849	-1755	-1418	-894
14.00	-67	953	2116	3084
15.00	3535	3237	2055	479
16.00	-1208	-2553	-3151	-2979
17.00	-2427	-1440	-724	5
18.00	414	755	780	1336
19.00	1355	1432	1230	915
20.00	804	584	204	-116
21.00	-535	-1149	-1872	-2140
22.00	-2238	-1806	-1194	-305
23.00	446	1150	1464	1607
24.00	1725	1745	1492	722
25.00	116	-486	-1123	-1379
26.00	-1338	-1258	-992	-795
27.00	-907	-374	-44	174
28.00	587	967	1090	1194
Middle camera distance (30 cm) Plate I-110-11				
6.00	2502	2301	1620	625
7.00	-558	-1555	-2415	-2651
8.00	-2533	-2197	-1571	-779
9.00	245	1317	2106	2426
10.00	2139	1477	601	-248

(continued)

Table 2. Continued.

s \ Δs	0.00	0.25	0.50	0.75
11.00	-565	-486	-289	-111
12.00	-189	-452	-864	-1337
13.00	-1409	-1389	-1133	-706
14.00	73	898	1833	2578
15.00	3006	2827	1915	437
16.00	-1169	-2250	-2685	-2638
17.00	-2090	-1284	-628	-150
18.00	159	479	708	834
19.00	808	919	957	791
20.00	739	597	464	203
21.00	-212	-529	-1266	-1673
22.00	-1793	-1347	-831	-337
23.00	354	831	1083	1381
24.00	1410	1318	1009	574
25.00	63	-302	-780	-1069
26.00	-1065	-1072	-812	-555
27.00	-603	-232	-113	326
28.00	431	708	915	857
29.00	906	885	543	213
30.00	-159	-231	-726	-962
31.00	-1121	-1012		
Short camera distance (12 cm) Plate I-214-24				
22.00	-1924	-1906	-1331	-594
23.00	342	892	1656	2090
24.00	2504	2362	2138	1523
25.00	403	-691	-1107	-1438
26.00	-1848	-1947	-1715	-1493
27.00	-1165	-600	45	389
28.00	655	1027	1357	1296
29.00	1304	1234	704	377
30.00	66	-486	-1080	-1305
31.00	-1393	-1323	-1189	-924
32.00	-693	-202	424	987
33.00	1119	1329	1398	984
34.00	870	684	99	-429
35.00	-609	-990	-1201	-1288
36.00	-1050	-575	-369	79
37.00	46	552	861	806
38.00	876	1012	904	470

(continued)

Table 2. Continued.

s \ Δs	0.00	0.25	0.50	0.75
39.00	21	-568	-774	-725
40.00	-994	-1363	-965	-437
41.00	-377	123	656	698
42.00	672	1240	1191	824
43.00	323	94	26	-100
44.00	-238	-582	-696	-667
Short camera distance (12 cm) Plate I-214-25				
22.00	-2425	-2103	-1595	-744
23.00	246	1181	1834	2154
24.00	2333	2090	1853	1139
25.00	132	-649	-1257	-1512
26.00	-1532	-1582	-1686	-1507
27.00	-874	-368	-5	433
28.00	773	1172	1382	1438
29.00	1489	1245	906	303
30.00	-159	-681	-1322	-1260
31.00	-1373	-1433	-1403	-884
32.00	-453	33	631	947
33.00	1262	1599	1628	1221
34.00	734	342	-53	-234
35.00	-577	-951	-880	-742
36.00	-831	-573	-118	-95
37.00	-20	442	1167	837
38.00	1024	1033	859	440
39.00	92	-282	-593	-644
40.00	-543	-856	-488	-393
41.00	-317	-21	137	335
42.00	685	651	664	656
43.00	595	219	125	92
44.00	-603	-796	-436	-567
Composite curve of 12, 30 and 75 cm data				
1.00	25	39	33	-8
2.00	-74	-164	-240	-272
3.00	-256	-203	-145	-130
4.00	-204	-371	-559	-607
5.00	-367	236	1109	1970
6.00	2476	2407	1703	613

(continued)

Table 2. Continued.

s \ Δs	0.00	0.25	0.50	0.75
7.00	-590	-1607	-2298	-2599
8.00	-2580	-2271	-1664	-757
9.00	373	1523	2355	2674
10.00	2364	1571	610	-186
11.00	-588	-601	-416	-258
12.00	-264	-516	-868	-1209
13.00	-1363	-1404	-1224	-812
14.00	-162	697	1656	2489
15.00	2921	2729	1896	602
16.00	-796	-1932	-2486	-2346
17.00	-1958	-1262	-590	-55
18.00	306	581	740	909
19.00	939	926	840	728
20.00	668	570	442	205
21.00	-209	-721	-1306	-1645
22.00	-1724	-1400	-900	-313
23.00	323	824	1179	1379
24.00	1457	1330	1048	609
25.00	76	-420	-813	-1011
26.00	-1051	-971	-803	-625
27.00	-482	-280	-55	200
28.00	457	696	862	920
29.00	909	787	524	241
30.00	-31	-380	-742	-935
31.00	-1020	-997	-834	-639
32.00	-172	166	494	700
33.00	805	863	805	658
34.00	452	213	-85	-315
35.00	-386	-652	-727	-660
36.00	-612	-374	-158	-6
37.00	8	323	661	535
38.00	619	666	574	296
39.00	37	-276	-444	-445
40.00	-499	-721	-472	-270
41.00	-226	33	257	335
42.00	442	614	603	481
43.00	299	102	49	-2
44.00	-275	-449	-368	-401

Table 3. Parameter values for N_2F_4. [a/]

	Trans-Gauche Mixture		Trans		Cardillo and Bauer Mixture	
	r, ℓ	2σ	r, ℓ	2σ	r, ℓ	Error
% Trans	71.2	8.1	100	0.010	53	3
% Gauche	28.8	7.7			47	3
r_{N-N}	1.492	0.007	1.495	0.006	1.489	0.004
r_{N-F}	1.372	0.002	1.372	0.002	1.375	0.004
$r_{F_1F_2}$	2.148	0.009	2.160	0.005		
$r_{N_1F_3}$	2.218	0.005	2.214	0.004		
$r_{F_1F_3(tr)}$	2.600	0.010	2.581	0.008		
$r_{F_1F_4(tr)}$	3.373	0.006	3.366	0.005		
$r_{F_1F_4(g)}$	2.487	0.042				
$r_{F_2F_4(g)}$	2.250	0.034				
$r_{F_1F_3(g)}$	3.365	0.007				
ℓ_{N-N}	0.048	0.005	0.048	0.004	0.044	0.004
ℓ_{N-F}	0.044	0.002	0.045	0.002	0.045	0.003
$\ell_{F_1F_2}$	0.064	0.004	0.066	0.004	0.053	0.004
$\ell_{N_1F_3}$	0.081	0.008	0.087	0.006	0.094	0.006
$\ell_{F_1F_3(tr)}$ [b/]	0.093	0.012	0.109	0.008	0.113	0.030
$\ell_{F_1F_4(tr)}$ [b/]	0.079	0.008	0.087	0.007	0.070	0.007
$\ell_{F_1F_4(g)}$ [b/]	0.093	0.012			0.120	0.030
$\ell_{F_2F_4(g)}$ [b/]	0.093	0.012			0.118	0.026
$\ell_{F_1F_3(g)}$ [b/]	0.079	0.008			0.068	0.012
$\angle F_1N_1F_2$	103.1°	0.6°	103.9°	0.4°	105.1° 102.9°	1.5° 1.0°
$\angle N_1N_2F_3$	101.4°	0.4°	101.0°	0.3°	100.1° 104.3° 100.6°	1.5° 1.0° 0.6°
θ (dihedral)	64.2°	3.7°	180°		67.1°	1.0°
RATIO [c/]	0.086		0.102			

[a/] Distances (r) and root-mean-square amplitudes (ℓ) in angstroms, angles in degrees. The r and ℓ values differ slightly from r_e (Hedberg and Iwasaki, 1964). The 2σ values include estimated of systematic as well as random error.

[b/] See text for constraints applied to these amplitudes.

[c/] RATIO $R = [\Sigma w_i \Delta_i^2 / \Sigma w_i I^2(obs)]^{1/2}$, where $\Delta_i = I_i(obs) - I_i(calc)$.

Table 4. Correlation matrix for trans-grauche N_2F_4.

% Trans	% Gauche	ℓ_{N-N}	ℓ_{N-F}	$\ell_{F_1F_2}$	$\ell_{N_1F_3}$	$\ell_{F_1F_3(tr)}$	$\ell_{F_1F_4(tr)}$	r_{N-N}	r_{N-F}
1.00	-0.99	0.02	0.29	0.22	0.13	0.33	0.54	0.25	0.14
	1.00	-0.01	-0.18	-0.18	-0.08	-0.30	-0.52	-0.16	-0.09
		1.00	0.38	0.02	0.00	0.01	0.01	0.01	-0.17
			1.00	0.19	0.26	0.22	0.21	0.55	0.25
				1.00	0.11	0.20	0.13	0.07	0.07
					1.00	0.60	0.11	0.18	0.11
						1.00	0.20	0.21	0.12
							1.00	0.18	0.10
								1.00	0.62
									1.00
1655.2[a]	1489.3	2.3139	0.1451	1.3078	7.7113	16.085	6.1076	6.0903	0.1211

$r_{F_1F_2}$	$r_{N_1F_3}$	$r_{F_1F_3(tr)}$	$r_{F_1F_4(tr)}$	$\angle F_1N_1F_2$	$\angle N_1N_2F_3$	θ [b]
0.39	-0.42	-0.69	-0.55	0.37	-0.51	-0.41
-0.36	0.47	0.66	0.55	-0.35	0.46	0.44
-0.01	0.01	-0.01	-0.02	0.02	0.02	-0.00
0.19	0.13	-0.24	-0.14	0.15	-0.42	0.04
0.13	-0.37	-0.38	-0.41	0.12	-0.31	0.04
0.87	0.32	-0.48	0.25	0.85	0.04	0.67
0.59	0.18	-0.39	0.08	0.57	-0.08	0.57
0.23	-0.20	-0.37	-0.29	0.21	-0.30	-0.19
0.10	0.27	0.22	-0.21	-0.01	-0.76	0.06
0.08	0.11	-0.12	-0.10	-0.09	-0.58	0.03
1.00	0.09	-0.72	0.05	0.99	-0.04	0.44
	1.00	0.55	0.88	0.07	0.41	0.59
		1.00	0.67	-0.69	0.56	0.07
			1.00	0.06	0.77	0.57
				1.00	0.06	0.43
					1.00	0.33
						1.00
10.195	2.2074	12.632	3.6821	46563.	20691.	1709180.

[a] Values of σ^2_{LS} (x 10^6). Distances and root-mean-square amplitudes in $Å^2$, angles in degrees^2.

[b] With the refinement procedure used, $\rho[\theta] = \rho[r_{F_1F_4(g)}] = -\rho[r_{F_2F_4(g)}] = \rho[r_{F_1F_3(g)}]$, and the respective values of σ^2_{LS} (x 10^6) are 223.79, 147.36, and 3.9220 $Å^2$.

Table 5. Correlation matrix for trans N_2F_4.

k[a]	ℓ_{N-N}	ℓ_{N-F}	$\ell_{F_1F_2}$	$\ell_{N_1F_3}$	$\ell_{F_1F_3}$	$\ell_{F_1F_4}$	r_{N-N}	r_{N-F}	$r_{F_1F_2}$	$r_{N_1F_3}$	$r_{F_1F_3}$	$r_{F_1F_4}$	$\angle F_1N_1F_2$	$\angle N_1N_2F_3$
1.00	0.03	0.73	0.07	0.37	-0.01	0.16	0.57	0.33	0.12	0.20	-0.12	-0.07	0.03	-0.41
	1.00	0.33	0.02	-0.01	0.00	0.00	-0.02	-0.21	-0.02	0.01	-0.00	-0.01	0.04	0.04
		1.00	0.06	0.24	-0.00	0.12	0.54	0.24	0.04	0.19	-0.08	-0.08	-0.02	-0.38
			1.00	-0.46	0.18	0.02	0.01	0.02	-0.29	-0.43	-0.18	-0.45	-0.28	-0.31
				1.00	-0.25	0.06	0.11	0.09	0.74	0.11	-0.36	0.07	0.69	-0.03
					1.00	0.01	-0.01	-0.00	-0.17	-0.20	-0.06	-0.20	-0.16	-0.13
						1.00	0.09	0.05	0.01	0.03	-0.02	-0.02	-0.00	-0.07
							1.00	0.60	-0.09	0.31	-0.06	-0.16	-0.24	-0.75
								1.00	-0.01	0.12	-0.04	-0.07	-0.26	-0.57
									1.00	-0.20	-0.67	-0.16	0.97	-0.05
										1.00	0.77	0.88	-0.23	0.39
											1.00	0.84	-0.64	0.59
												1.00	-0.14	0.75
													1.00	0.09
														1.00
50.767[b]	1.5361	0.0095	1.2260	2.6820	6.1944	4.2179	4.0309	0.0084	3.1282	1.5185	7.2757	2.4169	15564.	12917.

[a] Dimensionless scale constant of no structural significance. See Hedberg and Iwasaki (1964).

[b] Values of σ^2_{LS} (x 10^6). Distances and root-mean-square amplitudes in $Å^2$, angles in degrees^2.

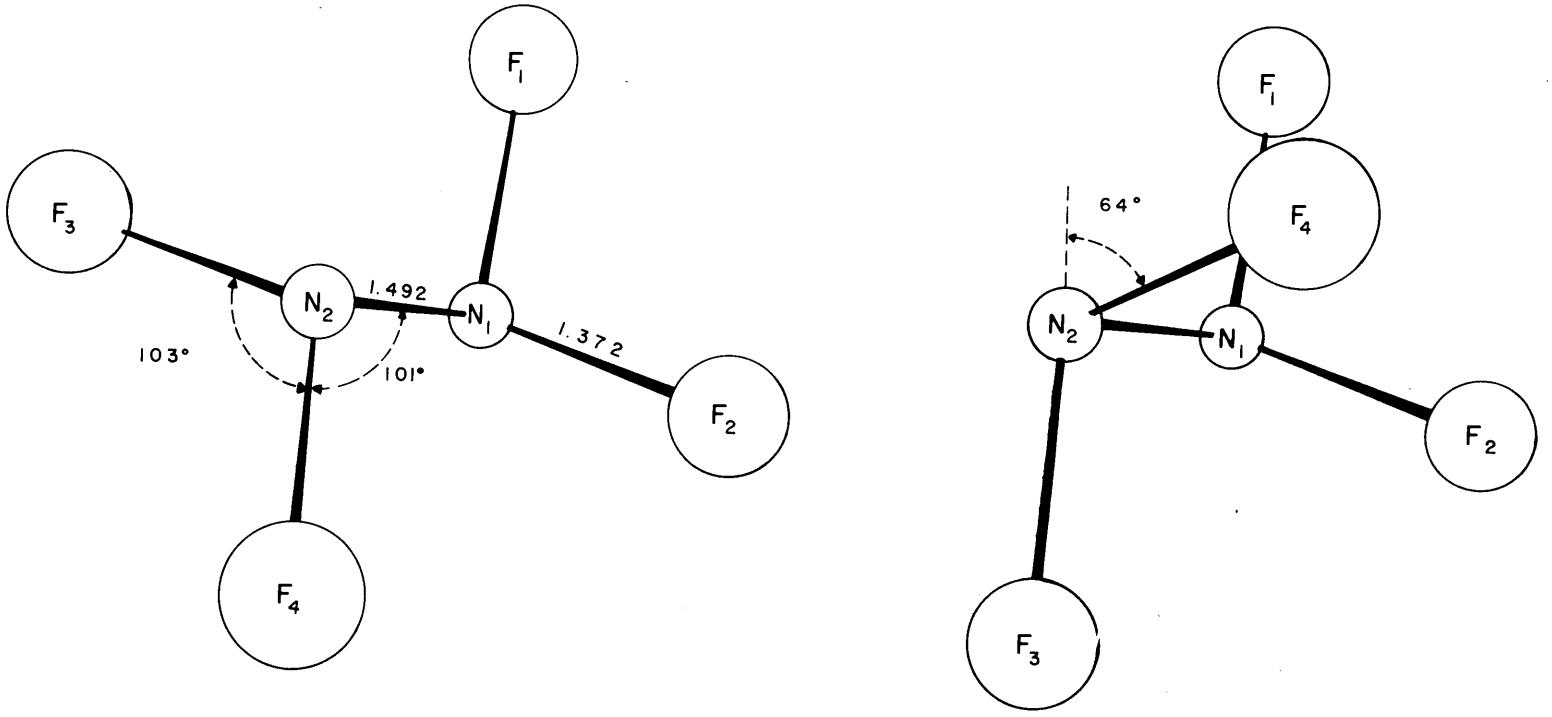

TRANS

GAUCHE

Figure 1. The two conformations of N_2F_4.

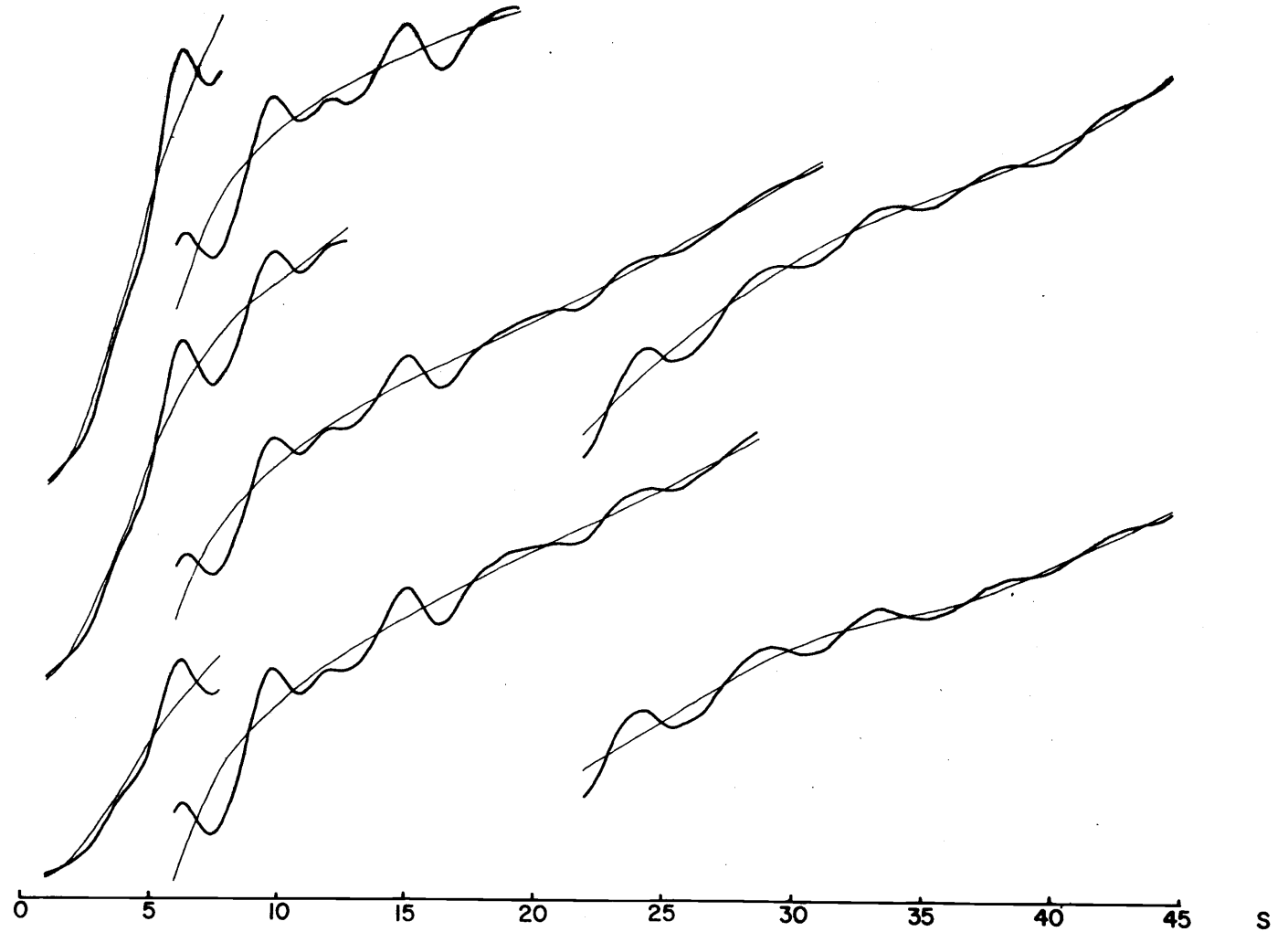

Figure 2. Sector corrected curves and final background curves for long, middle, and short sample-plate distances.

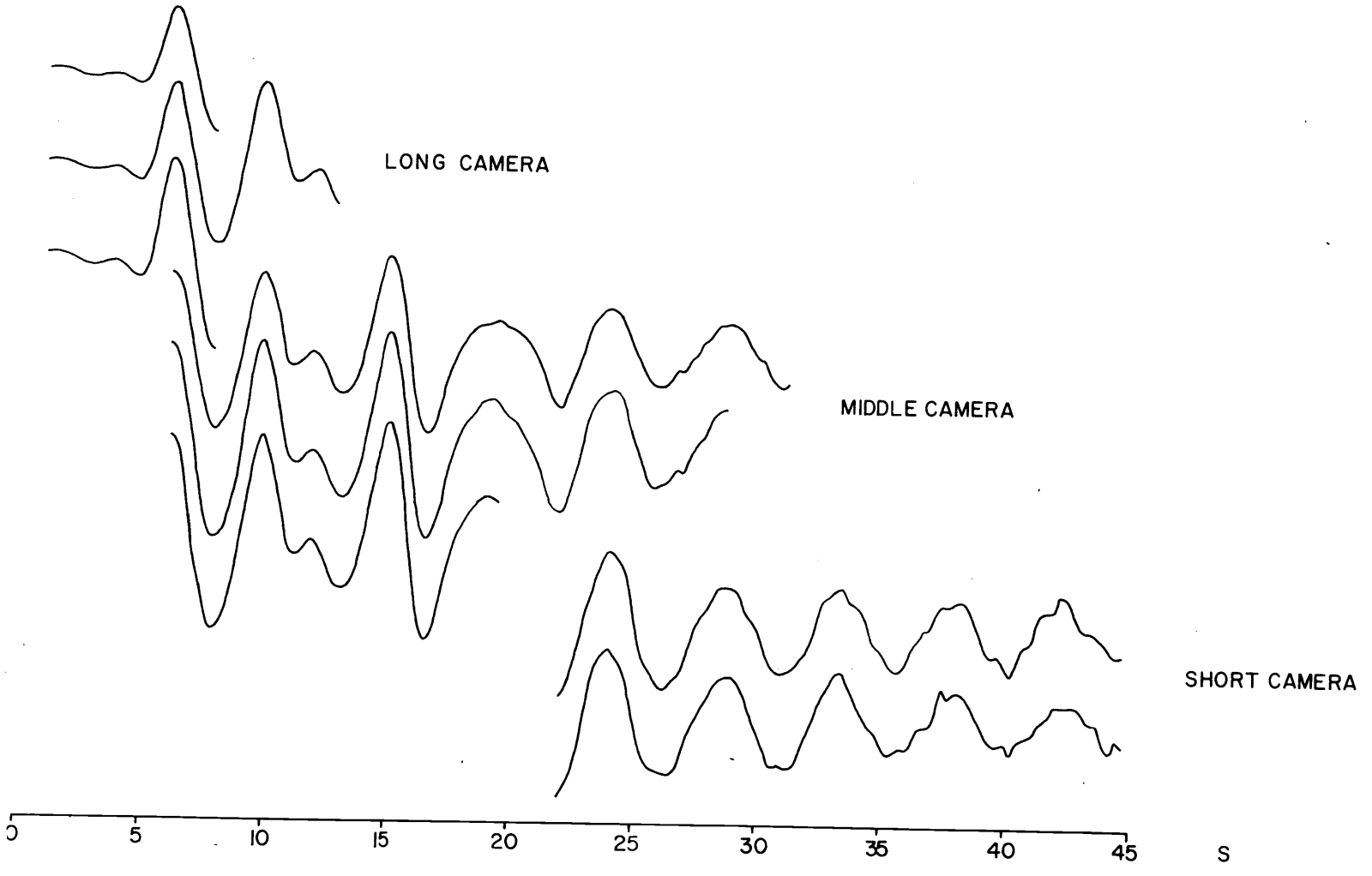

Figure 3. Experimental intensity curves $sI_m(s)$ for N_2F_4.

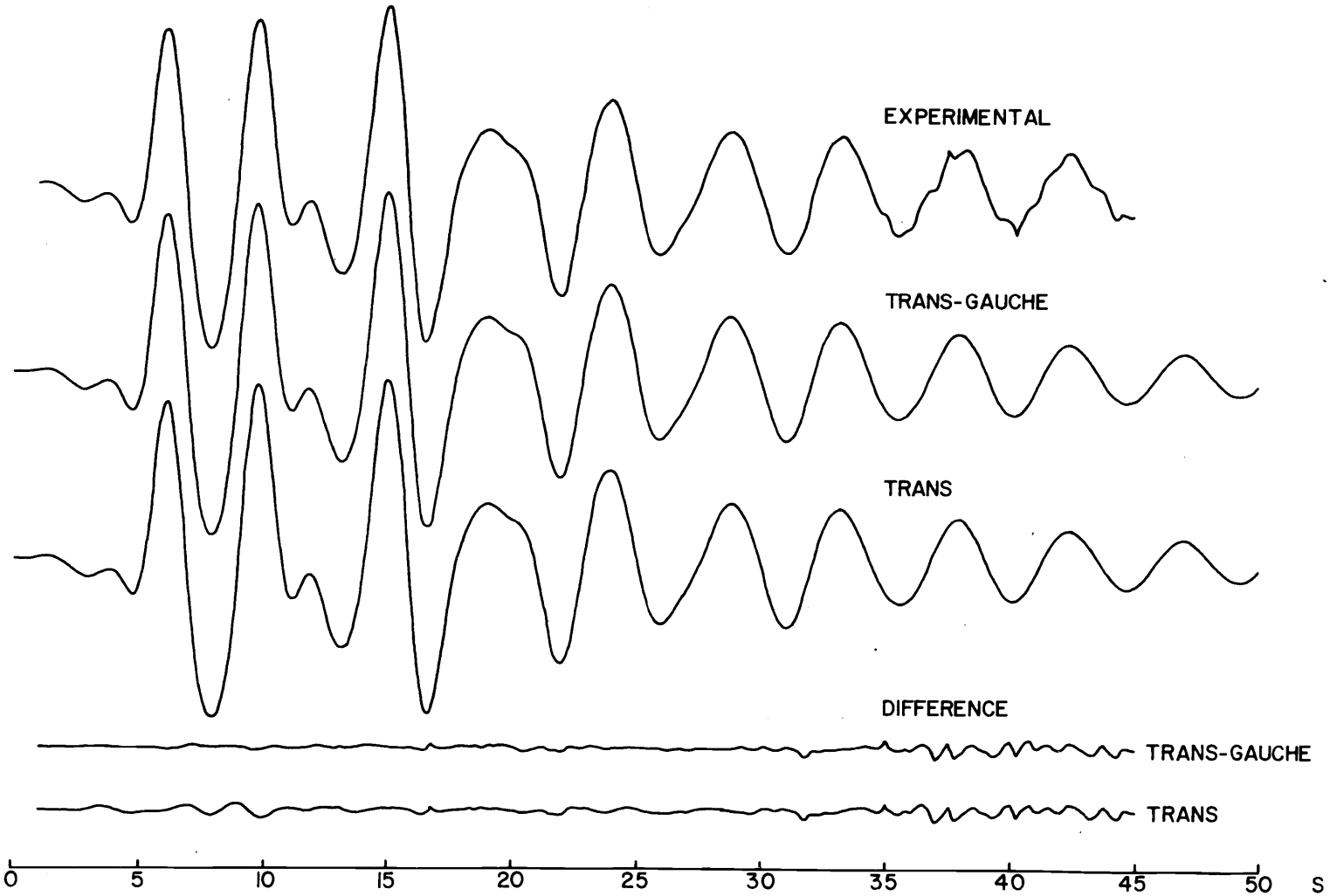

Figure 4. Intensity curves for N_2F_4. The experimental curve is a composite for three camera distances. The theoretical curves correspond to the models of Table 3. The difference curves are the experimental minus the theoretical.

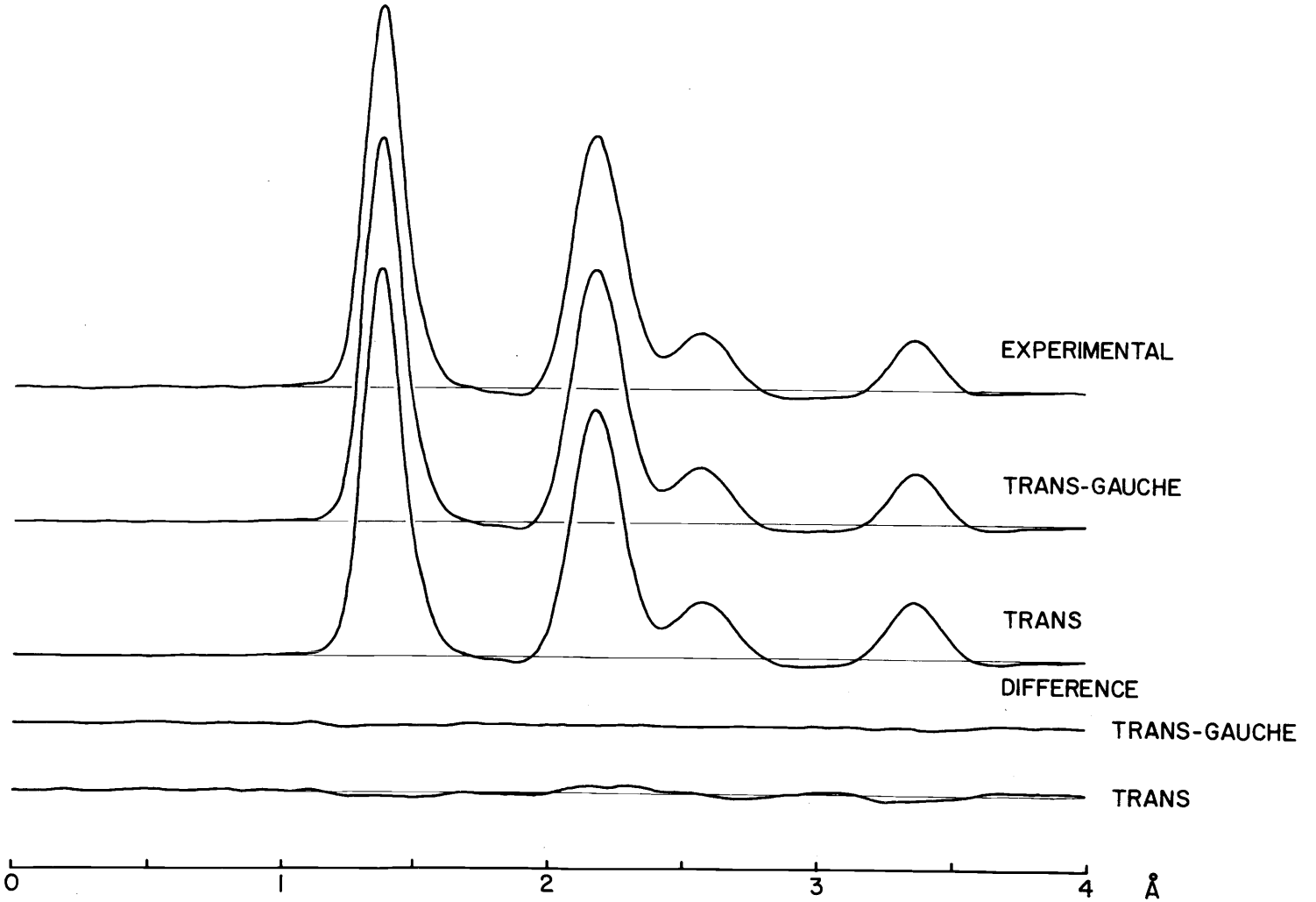

Figure 5. Radial distribution curves for N_2F_4. The experimental curve was calculated from the composite intensity curve. The theoretical curves were calculated from the intensity curves corresponding to the models of Table 3. The difference curves are the experimental minus the theoretical.

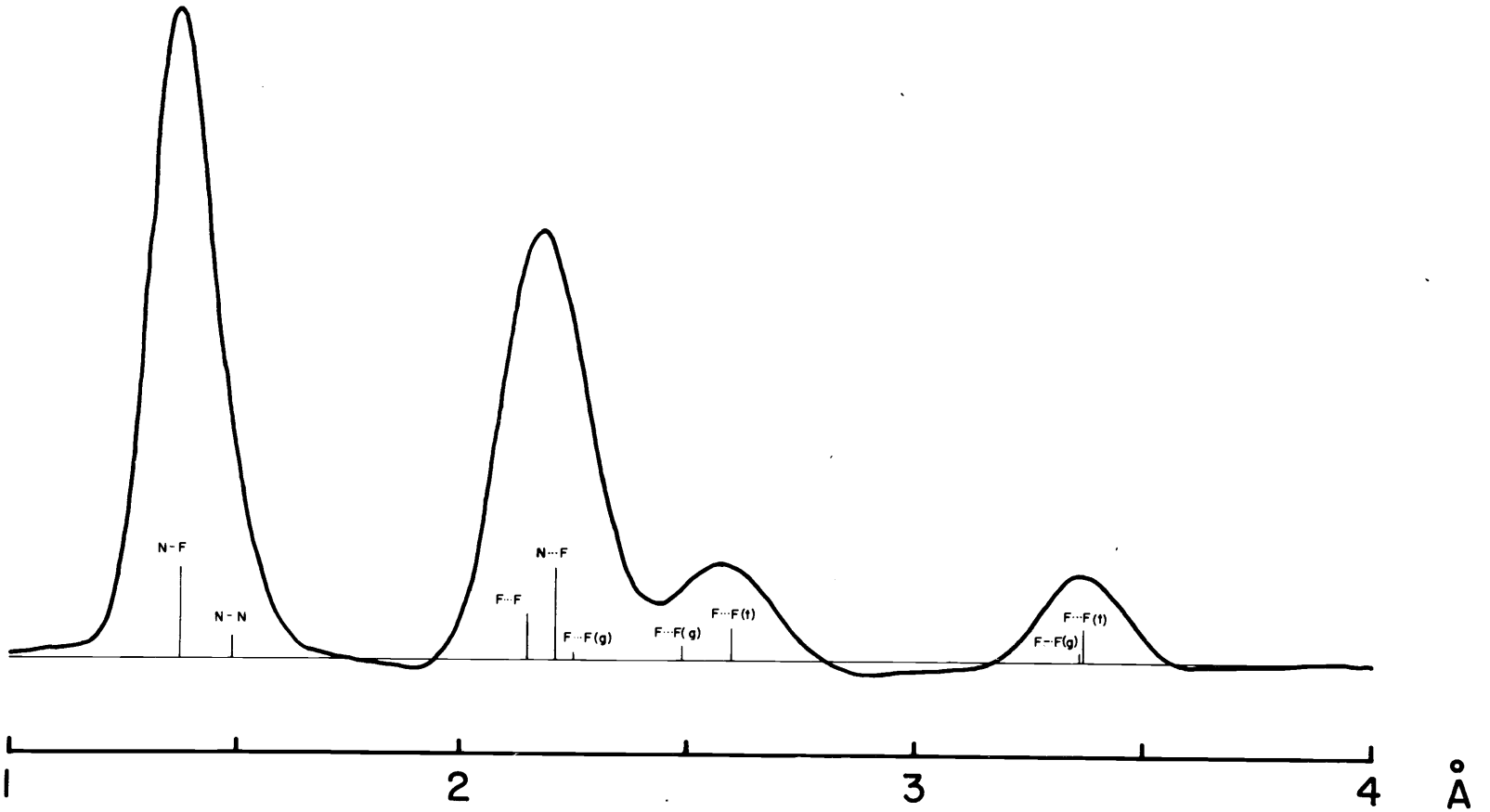

Figure 6. Experimental radial distribution curve for N_2F_4 showing the relative contributions for the different distances of the 71% trans/29% gauche model as given in Table 3.

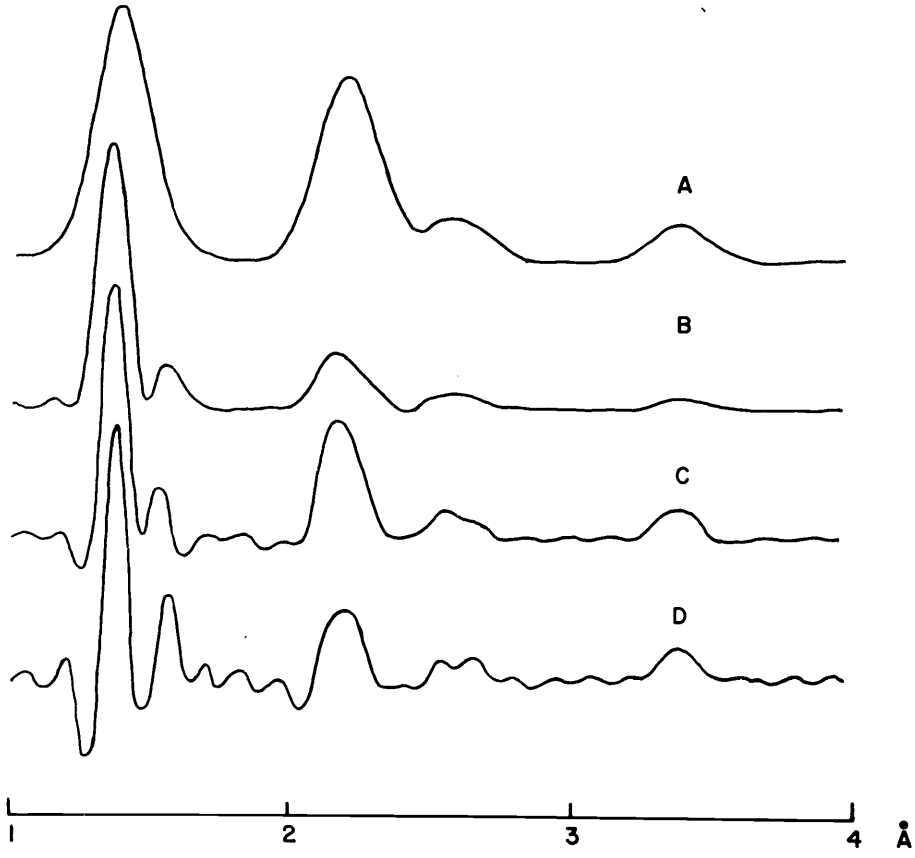

Figure 7. Experimental power spectra for N_2F_4. A: spectrum of averaged complex demodulates using a Tukey filter and $\tau_{max} = 42$. B: autocorrelation power spectrum using $\alpha = 0.02$ and $\tau_{max} = 40$. C: sharpened radial distribution curve using $\alpha = 0.03$. D: diagonal power spectrum using $\alpha = 0.03$ and $\tau_{max} = 10$.

BIBLIOGRAPHY

Bartell, L.S. (1955). J. Chem. Phys. 23, 1219.

Bohn, R.K. and S.H. Bauer. (1967). Inorg. Chem. 6, 304.

Brockway, L.O. (1936). Rev. Mod. Phys. 8, 231.

Cardillo, Mark J. and S.H. Bauer. (1969). Inorg. Chem. 8, 2086.

Colburn, Charles B. (1963). Advan. Fluorine Chem. 3, 92.

Colburn, Charles B., F.A. Johnson and Carolyn Haney. (1965). J. Chem. Phys. 43, 4526.

Cox, Hollace Lawton. (1967). Ph.D. Thesis. Indiana University.

Cox, H.L. and R.A. Bonham. (1967). J. Chem. Phys. 47, 2599.

Durig, J.R. and R.C. Lord. (1963). Spectrochim. Acta. 19, 1877.

Durig, James R. and James W. Clark. (1968). J. Chem. Phys. 48, 3216.

Fano, R.M. (1950). J. Acoust. Soc. Am. 22, 546.

Faxen, H. and J. Holtsmork. (1927). J. Zeits. f. Physik. 45, 307.

Glauber, Roy and Verner Schomaker. (1953). Phys. Rev. 89, 667.

Gundersen, Grete and Kenneth Hedberg. (1969). J. Chem. Phys. 51, 2500.

Hamilton, Walter Clark. (1964). Statistics in Physical Sciences. New York: Ronald Press.

Harmony, M.D., et. al. (1961). J. Chem. Phys. 35, 1129.

Hedberg, Kenneth and Machio Iwasaki. (1962). J. Chem. Phys. 36, 589.

Hedberg, Kenneth and Machio Iwasaki. (1964). Acta Cryst. 17, 529.

Hedberg, Lise. (1968). Unpublished data reduction program. Oregon State University.

Hedberg, L., R. R. Ryan and K. Hedberg. (1968). Unpublished least-squares program. Oregon State University.

Hoffman, C. J. and R. G. Neville. (1962). Chem. Rev. 62, 1.

Iwasaki, Machio, F. N. Fritsch and Kenneth Hedberg. (1964). Acta Cryst. 17, 533.

Jenkins, G. M. and D. G. Watts. (1968). Spectral Analysis and its Applications. San Francisco: Holden-Day.

Karle, J. and R. A. Bonham. (1964). J. Chem. Phys. 40, 1396.

Kaufman, Joyce J. (1962). J. Chem. Phys. 37, 759.

Koster, D. F. and Foil A. Miller. (1968). Spectrochim. Acta. 24A, 1487.

Kotov, Yu. I. and V. M. Tatevskii. (1963). Opt. i Spektroskopiya. 14, 443.

Lide, David R. and D. E. Mann. (1959). J. Chem. Phys. 31, 1129.

McClelland, B. W. and Kenneth Hedberg. (1971). To be published.

Mott, N. F. and H. S. W. Massey. (1965). The Theory of Atomic Collisions. London: Oxford University.

Oskam, A. R. Elst and J. C. Duinker. (1970). Spectrochim. Acta. 26A, 2021.

Pankratov, A. V. (1963). Russ. Chem. Rev. 32, 157.

Peacher, J. (1965). Ph. D. Thesis. Indiana University.

Ryan, R. R. and Kenneth Hedberg. (1969). J. Chem. Phys. 50, 4986.

Schroeder, M. R. and B. S. Atal. (1962). J. Acoust. Soc. Am. 34, 1679.

Seip, Hans M. (1967). Selected Topics in Structure Chemistry. Ed. by P. Andersen, O. Bastiansen and S. Furberg. Oslo: Universitetsforlaget.

Sheridan, J. and W. Gordy. (1950). Phys. Rev. 79, 513.

Schiff, L. I. (1955). Quantum Mechanics. New York: McGraw-Hill.

Traetteberg, Marit. (1964). J. Am. Chem. Soc. 86, 4265.

Traetteberg, M. and R. A. Bonham. (1965). J. Chem. Phys. 42, 587.

Yamaguchi, Akiko, et. al. (1959). J. Chem. Phys. 31, 843.

APPENDIX

COMPUTATIONAL FORMULAS FOR RADIAL DISTRIBUTION AND POWER SPECTRA FUNCTIONS

1. Radial distribution function, $D(r)$.

$$D(r) = \frac{\Delta s}{\sqrt{2\pi}} \sum_{s=S_{min}}^{S_{max}} I(s) \exp(-Bs^2) \sin(rs),$$

where B is the damping constant.

2. Sharpened radial distribution function, $SRD(r)$.

$$SRD(r) = \sqrt{2a}\ \Delta s \sum_{s=S_{min}}^{S_{max}} I(s) \exp[-a(S_{max}-s)] \sin(rs),$$

where a is the anti-damping constant.

3. Autocorrelation power spectrum, $APS(r)$. An autocorrelation function is first computed according to the formula:

$$A(\tau) = 2a\,\Delta s \sum_{s=S_{min}}^{S_{max}} I(s)I(s-\tau) \exp[-2a(S_{max}-s)].$$

The autocorrelation power spectrum is them computed as the cosine Fourier transform of $A(\tau)$:

$$APS(r) = 2\Delta\tau \sum_{\tau=0}^{\tau_{max}} A(\tau) \exp(-a\tau) \cos(r\tau).$$

4. Diagonal power spectrum, DPS(r). For every r-value a test function is computed according to the formula:

$$t(s) = C \sin(rs) \quad \text{for} \quad S_{min} \leq s \leq S_{max},$$

where C is a constant. The cross correlation function than can be defined for the test function and the experimental intensity function is computed as follows:

$$CR(\tau) = 2\alpha \Delta s \sum_{s=\tau}^{S_{max}} I(s)t(s-\tau) \exp[-2\alpha(S_{max}-s)].$$

For the same r-value for which the test function was computed, one point on the diagonal power spectrum is computed as follows:

$$DPS(r) = 2\Delta\tau \sum_{\tau=0}^{\tau_{max}} CR(\tau) \exp(-\alpha\tau) \cos(r\tau).$$

5. Average complex demodulate spectrum. For each s in the range $s = N-1, N, N+1, \ldots, S_m-N$ where $2N-1$ is the filter length. The real and imaginary components of the complex demodulates are calculated as:

$$Re(Z) = \sum_{\tau=1-N}^{N-1} w_\tau I(s-\tau) \cos[r(s+\tau)],$$

$$\mathrm{Im}(Z) = \sum_{\tau=1-N}^{N-1} w_\tau I(s-\tau)\, \sin[r(s+\tau)].$$

These values for all s are then averaged to form the spectrum for a particular value of r by

$$C(r) = \frac{1}{S_m - 2(N-1)} \sum_{N-1}^{S_m - N} [\mathrm{Re}(Z)^2 + \mathrm{Im}(Z)^2]^{1/2}.$$

This process is repeated for each r-value of interest.